Alexandria Engineering Journal (2023) 62, 1–15

HOSTED BY

Alexandria University

Alexandria Engineering Journal

www.elsevier.com/locate/aej
www.sciencedirect.com

Brownian motion and thermophoretic diffusion impact on Darcy-Forchheimer flow of bioconvective micropolar nanofluid between double disks with Cattaneo-Christov heat flux

Arfan Shahzad [a,b], Muhammad Imran [a], Madeeha Tahir [c], Shan Ali Khan [c], Ali Akgül [d], Sherzod Abdullaev [e], Choonkil Park [f], Heba Y. Zahran [g,h,i], Ibrahim S. Yahia [g,h,i]

[a] *Department of Mathematics, Government College University, Faisalabad 38000, Pakistan*
[b] *Department of Sciences & Humanities, National University of Computer and Emerging Sciences, Chiniot-Faisalabad Campus, 38000, Pakistan*
[c] *Department of Mathematics, Government College Women University, Faisalabad 38000, Pakistan*
[d] *Siirt University, Art and Science Faculty, Department of Mathematics, 56100 Siirt, Turkey*
[e] *Independent Researcher and CEO of the Company "Editory" LTD, Independent Researcher, Andijan Machine-Building Institute, Uzbekistan*
[f] *Research Institite for Natural Sciences, Hanyang University, Seoul 04763, Republic of Korea*
[g] *Laboratory of Nano-Smart Materials for Science and Technology (LNSMST), Department of Physics, Faculty of Science, King Khalid University, P.O. Box 9004, Abha 61413, Saudi Arabia*
[h] *Research Center for Advanced Materials Science (RCAMS), King Khalid University, P.O. Box 9004, Abha 61413, Saudi Arabia*
[i] *Nanoscience Laboratory for Environmental and Biomedical Applications (NLEBA), Semiconductor Lab, Department of Physics, Faculty of Education, Ain Shams University, Roxy, Cairo 11757, Egypt*

Received 22 March 2022; revised 2 July 2022; accepted 16 July 2022
Available online 29 July 2022

KEYWORDS

Bioconvection;
Cattaneo-Christov Heat flux;
Micropolar Nanofluid;
Stretching disks

Abstract The topic of fluid flow through disks is important due to a broad range of its applications in industries, engineering, and scientific fields. The objective of the current article is to analyze the bioconvective micropolar nanofluid flow between the coaxial, parallel, and radially stretching double disks in the occurrence of gyrotactic motile microorganisms with convective thermal boundary conditions. Darcy–Forchheimer medium is considered between the double disks that allow the flow horizontally with additional effects of porosity and friction. The flow is also considered under the impacts of thermal conductivity and thermal radiations. The influence of gyrotactic microorganisms is accommodated through the bioconvection, which increases the strength of thermal transportation. Furthermore, the Cattaneo-Christov heat flux theory is also accounted. The flow model is trans moved into a system of ordinary differential equations (ODEs) utilizing appropriate similarity

E-mail addresses: baak@hanyang.ac.kr (C. Park), heldemardash@kku.edu.sa (I.S. Yahia)
Peer review under responsibility of Faculty of Engineering, Alexandria University.

https://doi.org/10.1016/j.aej.2022.07.023
1110-0168 © 2022 THE AUTHORS. Published by Elsevier BV on behalf of Faculty of Engineering, Alexandria University
This is an open access article under the CC BY-NC-ND license (http://creativecommons.org/licenses/by-nc-nd/4.0/).

Nomenclature

C	Concentration of nanoparticles, $molL^{-1}$	N_1	Microorganism concentration at the lower disk
C_f	Skin friction coefficient	N_2	Microorganism concentration at the upper disk
C_1	Concentration of nanoparticles at the lower disk	Pe	Peclet number
C_2	Concentration of nanoparticles at upper disk	Pr	Prandtl number
u_r, u_z	Partial derivatives of u w.r.t r and z	u, v, w	Velocity vectors
D	Microorganisms' diffusion coefficient, m^2s^{-1}	W_c	Maximum cell swimming speed
D_B	Brownian diffusion coefficient, m^2s^{-1}	C_P	Specific heat at constant pressure
D_m	Microorganisms' diffusivity, m^2s^{-1}	Nc	bioconvection Rayleigh number
D_T	Thermophoresis diffusion coefficient, m^2s^{-1}	Nr	buoyancy ratio parameter
Lb	Bioconvection Lewis number	Rd	Thermal radiation parameter
Le	Lewis Number	r	Radius of disk, m
N	Density of microorganisms, m^{-3}	Nt	Thermophoresis number
Nb	Brownian diffusion parameter	Sn	Microorganisms' density number
g^*	Acceleration due to gravity, m^2s^{-1}	T	Temperature of fluid,K
W_c	Maximum cell swimming speed	θ	Dimensionless temperature
ϕ	Dimensionless volume fraction of nanoparticles	χ	Dimensionless microorganisms' density function
ζ	Similarity variable	ρ_f	Density of fluid, kgm^{-3}
ρ_m	Microorganism particles density	$(\rho c)_p$	Heat capacity of nanoparticles, $Jm^{-3}\ K^{-1}$
$(\rho c)_f$	Heat capacity of base fluid, $Jm^{-3}\ K^{-1}$	μ	Dynamic viscosity of nanoliquid, Nsm^{-2}
λ	Mixed convection parameter	γ	Stretching ratio parameter
j	microinertia density	β'	Thermal expansion coefficient
γ^*	Average volume of the microorganism	p	Pressure

transformation functions. The bvp4c technique has been used to solve the transformed flow model. The implication of some prominent physical and bioconvection parameters on velocities, microrotation, thermal field, volumetric concentration of nanoparticles, and microorganisms' fields are presented through graphs and tabular ways. It is observed that the stretching ratio parameter of the disks accelerates the axial and micro rotational velocities of the nanofluid. In contrast, the stretching Reynolds number slows down the radial velocity near the plane's center. The temperature profile goes high against the Brownian motion, thermal radiation, and thermal conductivity parameters, while an inverse trend has been observed for increasing magnitudes of Prandtl number. The nanoparticles concentration profile is upsurged against the thermophoresis parameter. The density profile of gyrotactic motile microorganisms is de-escalated by the Peclet number and the bioconvection Lewis number. Micropolar parameters cause an increase of couple stresses and a decrement in shear stresses. A comparison with published work is provided under certain limitations to test the validity of numerical scheme accuracy.

© 2022 THE AUTHORS. Published by Elsevier BV on behalf of Faculty of Engineering, Alexandria University This is an open access article under the CC BY-NC-ND license (http://creativecommons.org/licenses/by-nc-nd/4.0/).

1. Introduction

The fluid flow through the parallel disks has critical role in both theoretical and practical considerations, particularly in the chemical mechanical engineering processes such as air cleaning machines, turbine machinery, centrifugal pumps, metal pumping, jet motors, electric power generating systems, manufacturing of thin plastic sheets, insulating materials, and paper fabrication. The study of the heat transfer phenomenon in the presence of thermal radiation and thermal conductivity has also achieved great attention from scientists in recent decades. The impact of thermal radiation at larger temperatures cannot be denied as it encountered a variety of exciting applications in power generation, missiles technology, semiconductor wafers, etc. Some recent findings are discussed in [1–5].

Micro-polar fluids are fluids that correlate the macroscopic velocities field with particle rotation. Solid particles suspended in a viscous medium make up these fluids. Ferrofluid, bubbly fluids, and blood fluid flows are examples of micro-polar fluid flows. Micro-polar flow fluids are employed in various industrial applications, including polymeric solutions, lubricating fluids, and biologic constructions. Micro-polar fluids have been studied by a number of scientists from all over the world. The major inspiration of micropolar fluid was introduced by Eringen [6]. Ashraf *et al.* [7] scrutinized micropolar fluid flow between dual disks. Ashraf *et al.* [8] computed MHD flow and thermal transportation of micropolar fluid among dual porous disks. Ali *et al.* [9] examined the effect of MHD on micropolar fluid through double disks. The magnetohydrodynamic micropolar dusty nanofluid in the porous medium was

analyzed by Ghadikolaei *et al*. [10]. Taylor *et al*. [11] studied the impact of the free convectional flow of micropolar fluid through the sheet. Nadeem *et al*. [12] illustrated the micropolar fluid flow among dual parallel disks. Kumar *et al*. [13] examined the simultaneous solutions for the first and second order slip conditions on micropolar fluid flow through a convective surface in the occurrence variable heat source/sink. Anantha *et al*. [14] analyzed the significance of viscous dissipation on magnetized micropolar fluid past a slendering stretching surface with modified heat flux model. Venkata *et al*. [15] studied the effect of Soret and Dufour on magnetohydrodynamic Casson fluid flow over a stretching surface with convective–diffusive conditions. Sandeep *et al*. [16] investigated the effect of nonlinear radiation on MHD flow of hybrid nanofluid with heat source effect. Kumar *et al*. [17] introduced the physical characteristics on magnetohydrodynamic micropolar fluid flow over an exponentially stretching curved surface. Some latest work is also discussed in [18–20].

Nanofluid characteristics, particularly low conductivity, and appropriate thermophysical properties, are essential in research. Maintaining, sustaining, and developing technological items such as laptops, computers, electronic components, high-powered wavelengths, and motor generators are highly beneficial in various industrial methodologies. For this purpose, nanofluids have shown promise in increasing manufacturing productivity and findings. Nanotechnology is an exciting field of science. The ideas that prompted nanotechnology were first explored in 1959 by renowned scientist Richard Feynman in his speak. There are Plenty of Room at the Bottom, in which he explained the possibility of synthesizing through direct manipulation of molecules [21]. Nanofluids involve suspended nanoparticles with sizes less than 1–100 nm, which improve thermal conductivity. Nanofluids have various implementations in heating water, transportation improvement, heat transfer performance of refrigerators as well as chillers, and optimized solar power absorption. Nanofluids are utilized to cool machines, nuclear power stations, transformer fuel, and microprocessors. These are also utilized in the administration of drugs delivery as well as radiation to physicians. Choi [22] is associated with the first advanced work in this field, paving the idea for scientists to scrutinize nanofluids. Buongiorno [23] discussed the transfer properties of nanofluids. He developed a method known as the seven-slip framework, which parallelizes the velocity of the base liquid as well as nanoparticles. Waqas *et al*. [24] disclosed the effect of radiative nanofluid flow. Rauf *et al*. [25] investigate the swirling flow of the Maxwell fluid model through disk.

Heat transfer phenomena are of course given great importance in scientific and industry sectors such as marine engineering, thin-film technology, nanotechnology, and military sectors. In the present technical age, the demand for beneficial heat phenomena in enhancing heat proficiency has been improved. Heat conduction has been studied over the past two centuries as a means of heat transportation. The Cattaneo modified Fourier's law to include thermal relaxation time to overcome this difficult phenomenon. Heat transport mechanisms are important in different fields such as Space technology, furnace design, nuclear reactor, power plant, and biomedical fields. Rauf *et al*. [26] examined the swirling flow of Maxwell-over porous disk. Hayat *et al*. [27] illustrate the impact of Cattaneo-Christov heat and mass fluxes on the three-dimensional flow of viscoelastic nanofluid. Shehzad *et al*. [28] investigated Cattaneo-Christov double diffusion theory in micropolar nanofluid flow. Rauf *et al*. [29] reported the utilization of the Maxwell and Cattaneo laws for a micropolar non-Newtonian flow. Many researchers [30–33] discussed the Cattaneo-Christov heat/mass flux on nanofluids.

Microorganisms are multicellular organisms that exist in all living things, including animals, humans, as well as plants. Microorganisms produce bioconvection because they are much denser than water due to the aggregation of microorganisms. The bioconvection mechanism is demonstrated by oxytactic bacteria, where microorganisms swim. In reality, the bioconvection concept is associated with focused swimming cells, which are connected to microorganisms. Suspension of microorganisms (Oxytaxis, gravitaxis, gyrotaxis, etc.) in nanofluids improves their strength. The movements of microorganisms are microscopic in fluids. Microorganisms are also utilized in medicines such as antibiotics and aid to create vaccines. These particles are used on a wide scale of commercial and industrial product categories, such as biodiesel, ethanol, biofertilizer, etc.

The intriguing physiological significance of bioconvection has been successfully adjusted in biofuels production, ethanol, and a variety of manufacturing and environmental technologies. Other than that, nanoparticle bioconvection is connected to stratified density as well as pattern structure caused by the conversation of microorganisms, buoyancy forces, as well as nanoparticles. It is frequently identified that the existence of gyrotactic motile microorganisms improves the suspension consistency of nanoparticles. Many researchers have mentioned this fascinating concept in recent decades. Platt [34] first created the term "bioconvection" to describe a spontaneous procedure of improvement in the motion of swimming motile gyrotactic microorganisms. Kuznetsov [35] examined the isothermal convective principle using two distinct microorganisms, gyrotactic and oxytactic. Khan et al. [36] evaluated the rheological features of a Jeffrey nanofluid comprising gyrotactic motile microorganisms in an accelerating mode with the importance of activation energy and effectual Prandtl number. Hayat *et al*. [37] conducted the flow of magnetohydrodynamics (MHD) viscous liquid across a stretchable cylinder using nonlinear thermal radiation containing gyrotactic motile microorganisms. Abdelmalek *et al*. [38] proposed mathematical modeling for the unstable volatility finite flow of the upper layer produced by the horizontally rotational disk and transported by rate-type nanofluid in the existence of gyrotactic microorganisms.

This article investigates the Darcy-Forchheimer impacts in a micropolar nanofluid flow containing gyrotactic microorganisms between two coaxial, parallel, and radially stretching disks the presence of gyrotactic motile microorganisms with convective thermal boundary conditions. The effects of heat conductivity and thermal radiations are also considered for this flow. The influence of gyrotactic microorganisms is accommodated through the bioconvection. The nanofluid Buongiorno model is also used for the constitution of flow equations. The flow model is transformed into a system of ordinary differential equations by using some suitable similarity functions. This transformed flow model is then solved by the bvp4c method.

2. Formulation of flow problem

We consider a three-dimensional, steady, and incompressible flow of a micropolar nanofluid in the presence of gyrotactic motile microorganisms between two coaxial, parallel, and radially stretching disks. The upper and lower disks with stretching rates (S_2, S_1) are located at $z = h$ and$z = -h$, respectively. The nanofluid Buongiorno model is also used for the constitution of flow equations. Effects of thermal conductivity and thermal radiations are significant in modeling the energy equation (5) while the concentration of motile microorganisms is deliberated through equation (7). The velocity components and microrotation fields are denoted by (u, v, w) and$\left(0, \tilde{v}, 0\right)$, respectively. The thermal and solute impacts of nanoparticles and the concentration of microorganisms at an upper disk are represented byT_2, C_2, and N_2 while on lower diskT_1, C_1, andN_1, respectively. Under the above consideration, governing flow equations are [39,40]:

$$u_r + \frac{u}{r} + w_z = 0 \tag{1}$$

$$\rho_f(uu_r + wu_z) = -\partial_r(p) + k\,\tilde{v}_z - (k+\mu)\left(\tfrac{u}{r^2} - \tfrac{u_r}{r} - u_{rr} - u_{zz}\right) - Fu^2 + \tfrac{1}{\rho_f}\left[\rho_f\beta^{**}g^*(1-C_f)(T-T_\infty) - (\rho_p-\rho_f)g^*(C-C_\infty) - g^*\gamma^*(\rho_m-\rho_f)(N-N_\infty)\right] \tag{2}$$

$$\rho_f(uw_r + ww_z) = -\partial_r(p) + k\left(\tilde{v}_r + \frac{\tilde{v}}{r}\right) - (k+\mu)\left(\frac{w}{r^2} - \frac{w_r}{r} - w_{rr} - w_{zz}\right) \tag{3}$$

$$\rho_f j\left(u\tilde{v}_r + w\tilde{v}_z\right) = -2k\,\tilde{v} + k(u_z - w_r) - \tilde{\gamma}\left(\frac{\tilde{v}}{r^2} - \frac{\tilde{v}_r}{r} - \tilde{v}_{rr} - \tilde{v}_{zz}\right) \tag{4}$$

$$uT_r + wT_z = \tfrac{K(T)}{r}T_r + \partial_r(K(T)(T_r)) + \partial_z(K(T)(T_z)) - \gamma_1^*[u^2T_{rr} + w^2T_{zz} + 2uwT_{rz} + T_r(uu_r + ww_z) + T_z(uw_r + ww_z)] + \tau\left[D_B(C_rT_r + C_zT_z) + \tfrac{D_T}{T_m}\left\{(T_r)^2 + (T_z)^2\right\}\right] + \tfrac{16\sigma^*T_{2h}^3}{3k^*(\rho c)_p}T_{zz}, \tag{5}$$

$$uC_r + wC_z = \frac{k}{\rho c_p}\left(C_{rr} + \frac{1}{r}C_r + C_{zz}\right) + \frac{D_T}{T_m}\left(T_{rr} + \frac{1}{r}T_r + T_{zz}\right), \tag{6}$$

$$uN_r + wN_z = D_m\left(N_{rr} + \frac{1}{r}N_r + N_{zz}\right) - \frac{bW_c}{(C_1-C_2)}C_zN_z - \frac{bW_c}{(C_1-C_2)}NC_{zz}, \tag{7}$$

with the boundary conditions [40,41].

$$\begin{cases} u = S_1 r,\ w = 0,\ k_{nf}\frac{\partial T}{\partial z} = -h_1(T_1 - T),\ C = C_1,\ N = N_1 \ at\ z = -h \\ u = S_2 r,\ w = 0,\ k_{nf}\frac{\partial T}{\partial z} = -h_2(T - T_2),\ C = C_2,\ N = N_2 \ at\ z = h \end{cases} \tag{8}$$

where T denotes the temperature, C be the concentration of nanoparticles, N is the microorganisms density, $F = c_b/\tilde{K}^{1/2}$ is the non-uniform inertia (drag force) coefficient, ρ_f signifies the fluid density, ρ_p denotes the nanoparticles density, k denotes the vortex viscosity, ρ_m is the density of microorganism, j indicates the microinertia density, β' is the coefficient of thermal expansion, g^* signifies the gravity, γ^* is the average volume of the microorganism, p be the pressure, μ designates the dynamic viscosity, c_p is the specific heat, $\tilde{\gamma}$ is the spin gradient viscosity, γ_1^* is the thermal relaxation time, D_B indicates the coefficient of Brownian motion, D_T is the thermophoresis diffusion parameter, T_m be the mean fluid temperature, D_n be the coefficient of microorganisms diffusion, Wc is the cell's maximum swimming speed, b is the chemotaxis constant, S_1 be the stretching rate at lower disk, S_2 denotes upper disk stretching rate, r is the radius of disk, and (h_1, h_2) are the convective heat transfer coefficients at lower and upper disks, respectively. The term $\frac{16\sigma^*T_{2h}^3}{3k^*}$ in equation (5) depicts the thermal radiative heat transfer and $K(T)$ indicates the temperature dependent thermal conductivity defined as$K(T) = k_0(1 + \varepsilon(T - T_2)/(T_1 - T_2))$, where k_0 and ε is the thermal conductivity parameters.

The following similarity transformations are applied to reduce the system of PDEs to ordinary differential equations [40,41].

$$\begin{cases} u = -\frac{1}{2}rS_1f'(\zeta),\ w = \tilde{a}\,S_1f(\zeta),\ \tilde{v} = -\frac{1}{2}\frac{rS_1}{\tilde{a}}g(\zeta) \\ \theta(\zeta) = \frac{T-T_2}{T_1-T_2},\ \phi(\zeta) = \frac{C-C_2}{C_1-C_2},\ \chi(\zeta) = \frac{N-N_2}{N_1-N_2},\ where\ \zeta = \frac{z}{\tilde{a}} \end{cases} \tag{9}$$

The continuity equation (1) is satisfied under (9) and equations (2)–(7) after eliminating the pressure term are transformed into the following equations:

$$(a_1+1)f^{(iv)} - Reff''' - F_rf'^2 - a_1g'' + \lambda(\theta - Nr\phi - Nc\chi) = 0, \tag{10}$$

$$a_1f' - a_2Re\left(g'f - \frac{1}{2}gf'\right) + a_3g' - 2a_1g = 0, \tag{11}$$

$$\theta''\left(2 + \frac{4}{3}Rd + \varepsilon\theta\right) + \varepsilon\theta'^2 - RePr(\gamma_1(f^2\theta'' + ff'\theta') + f\theta') + Pr\theta'(Nt\theta' + Nb\phi') = 0, \tag{12}$$

$$\phi'' - ReSc(f\phi') + \frac{Nt}{Nb}\theta'' = 0, \tag{13}$$

$$\chi' - \chi'(LbRef + Pe\,\phi') - Pe\,\phi'(\chi + N_\delta) = 0. \tag{14}$$

The Boundary conditions (8) are also converted into the following.

$$\begin{cases} f(-1) = f(1) = 0,\ f'(-1) = -2,\ f'(1) = -2\gamma, \\ g(-1) = g(1) = 0, \\ \theta(-1) = \frac{-1}{A}Bi_1(1 - \theta(-1)),\ \theta(1) = \frac{-1}{A}Bi_2\theta(1),\ \phi(-1) = 1, \\ \phi(1) = 0,\ \chi(-1) = 1,\ \chi(1) = 0 \end{cases} \tag{15}$$

where $a_1 = k/\mu$ be the vortex viscosity parameter, $a_2 = \tilde{\gamma}/a^2\mu$ designates the spin gradient viscosity parameter, $a_3 = j/a^2$ is the microinertia density parameter, $\lambda = \beta'g^*T_2(1 - C_2)/a(\rho c)_f$ be the mixed convection parameter, $Nr = (\rho_p - \rho_f)(C_1 - C_2)/\beta'\rho_f(1 - C_f)(T_1 - T_2)$ is the Buoyancy ratio parameter, $Nc = \gamma^*(\rho_m - \rho_f)(N_1 - N_2)/\rho_f\beta'(1 - C_2)(T_1 - T_2)$

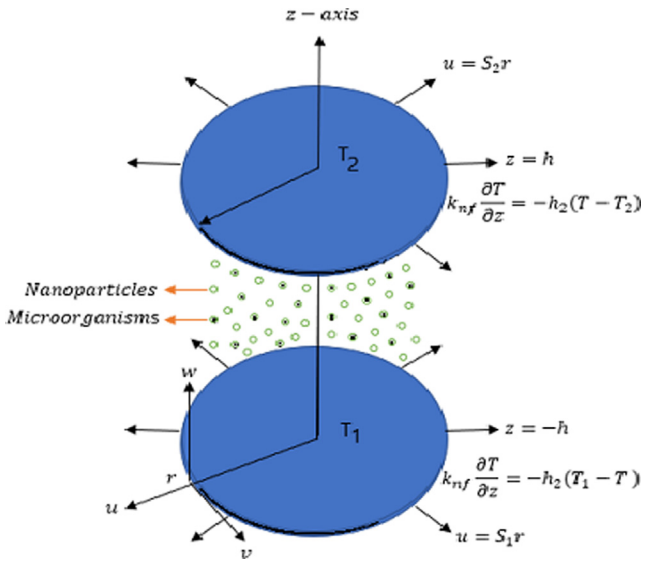

Fig. 1 The geometry of flow problem.

signifies the bioconvection Rayleigh number, $Fr = F.(rS_1 2h/\upsilon)$ is the non-dimensional inertia coefficient (Darcy-Forchheimer parameter), $\gamma_1 = \gamma_1^* S_1$ is the thermal relaxation time parameter, $Re = \rho S_1 h^2/\mu$ is the stretching Reynolds number, $Rd = 4\sigma T_{2h}^3/3kk^*$ is the thermal radiation parameter, $Pr = \mu c_p/k_0$ be the Prandtl number, $Nt = \tau D_T/\upsilon T_m.(T_1 - T_2)$ illustrates thermophoresis parameter, $Nb = \tau D_B/\upsilon.(C_1 - C_2)$ is the Brownian motion parameter, $Sc = \upsilon/D_n$ is the Schmidt number, $Lb = \nu_f/D_m$ be the bioconvection Lewis number, $Pe = bW_c/D_m$ defines the Peclet number, $N_\delta = N_2/N_1 - N_2$ is the microorganisms concentration difference parameter, $\gamma = S_1/S_2$ is the stretching ratio parameter, $A = k_{nf}/k_f$ is the thermal conductivity ratio parameter of nanofluid to the base fluid, and $Bi_1 = h_1 h/k_f$, $Bi_2 = h_2 h/k_f$ are the thermal Biot numbers for the lower and upper disks, respectively (see Fig. 1).

The engineering quantities of interest namely skin friction coefficient, local Nusselt number, local Sherwood number and local microorganisms' density number are describing as [35]:

$$C_f = -\tfrac{1+a_1}{2Re} f''(1), C_g = \tfrac{a_3}{2Re} g'(1), Nu_{r2} = -(1+Rd)\theta'(1), Nu_{r1} = -(1+Rd)\theta'(-1),$$
$$Sh_{r2} = -\phi'(1), Sh_{r1} = -\phi'(-1), Sn_{r2} = -\chi'(1), Sn_{r1} = -\chi'(-1), \tag{16}$$

3. Numerical algorithm

The coupled highly nonlinear ordinary differential equations (10)–(14) along with boundary constraints (15) is difficult to solve therefore such types of problems are solved numerically. In this article shooting scheme via bvp4c built-in function, MATLAB is used to compute the result of nonlinear ODEs numerically. For this firstly we reduce the order of equations by introducing some new variables, so let.

$$\begin{cases} f = p_1, f' = p_2, f'' = p_3, f''' = p_4, f^{(iv)} = p_4', \\ g = p_5, g' = p_6, g'' = p_6', \\ \theta = p_7, \theta' = p_8, \theta'' = p_8', \\ \phi = p_9, \phi' = p_{10}, \phi'' = p_{10}' \\ \chi = p_{11}, \chi' = p_{12}, \chi'' = p_{12}' \end{cases} \tag{17}$$

$$p_4^{(iv)} = \frac{1}{(a_1+1)}\left[Rep_1p_3 - F_rp_2 - a_1p_6' - \lambda(p_7 + Nrp_9 + Ncp_{11})\right], \tag{18}$$

$$p_6' = \frac{1}{a_3}\left[a_2 Re\left(p_1p_6 - \frac{1}{2}p_2p_5\right) + a_1(2p_5 - p_3)\right], \tag{19}$$

$$p_8' = \frac{\Pr p_8}{\left(2 + \frac{4}{3}Rd + \varepsilon_1 p_7 - Re\Pr\gamma_1 p_1^2\right)}\left[Re(\gamma_1 p_2 + 1)p_1 - (Ntp_8 + Nbp_{10}) - \frac{\varepsilon_1}{\Pr}p_8\right], \tag{20}$$

$$p_{10}' = Re.Sc.p_1p_{10} + \frac{Nt}{Nb}p_8', \tag{21}$$

$$p_{12}' = (LbRep_1 + Pe\,p_{10})p_{12} + Pe(p_{11} + N_\delta)p_{10}' \tag{22}$$

with the boundary conditions given in (15) as.

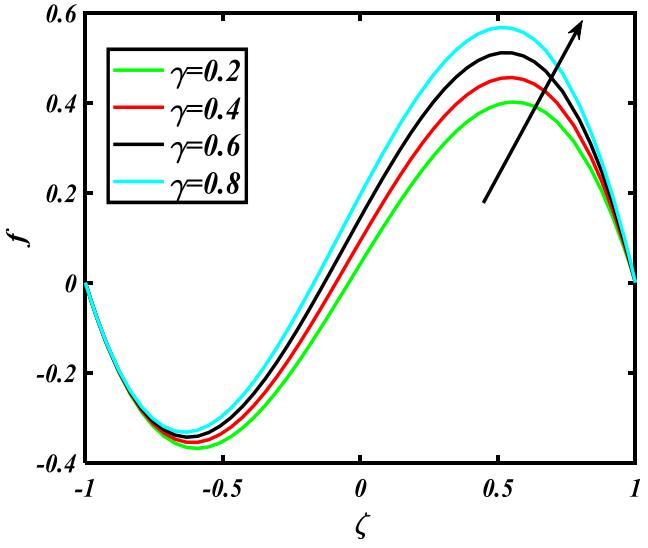

Fig. 2 Effect of γ on f.

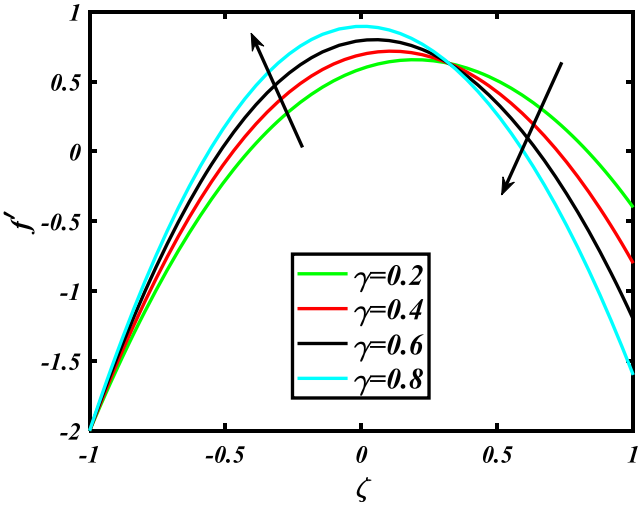

Fig. 3 Effect of γ on f'.

$$\begin{cases} p_1(-1) = p_1(1) = 0,\ p_2(-1) = -2,\ p_2(1) = -2\gamma,\ p_5(-1) = p_5(1) = 0, \\ p_7(-1) = \frac{-1}{A}\gamma_3(1 - p_7(-1)),\ p_7(1) = \frac{-1}{A}\gamma_4 p_7(1), \\ p_9(-1) = 1,\ p_9(1) = 0,\ p_{11}(-1) = 1,\ p_{11}(1) = 0. \end{cases} \tag{23}$$

4. Results and discussion

The transformed system of equation (10–14) with boundary constraints (15) are solved numerically by the bvp4c function on MATLAB using a famous mathematical shooting technique. This section is primarily concerned with the effects of some developing parameters on axial velocity$f(\zeta)$, radial velocity$f'(\zeta)$, and angular velocity$g(\zeta)$, the temperature field of nanomaterials$\theta(\zeta)$, the solutal field of species$\phi(\zeta)$, and the motile microorganism's profile$\chi(\zeta)$. With the aid of graphs and tabular data, the outcomes of dimensionless profiles are briefly scrutinized. The impacts of salient parameters of the flow fields are depicted in Figs. 2–21.

4.1. Axial, radial, and angular velocity distributions

Figs. 2–4 examine the significance of the stretching ratio parameter γ on the axial, radial, and angular velocities, respectively. Fig. 2 discloses the stimulation of axial velocity against the stretching ratio parameterγ. The axial velocity boosted up throughout the plane from upper to the lower disk with amplifying magnitudes of the stretching ratio parameter. In Fig. 3, the parabolic nature profile of radial velocity improves near the upper disk and reduces near the lower disk. At $\gamma = 1$(when $E_1 = E_2$), the symmetric profile is obtained, and profiles resem-

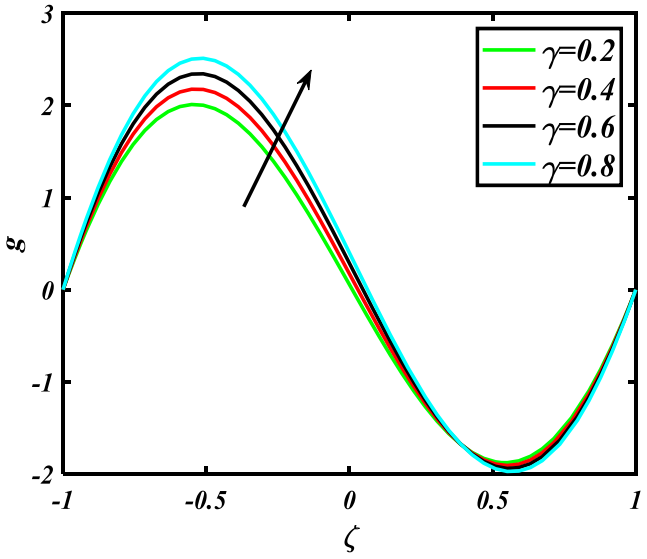

Fig. 4 Effect of γ on g.

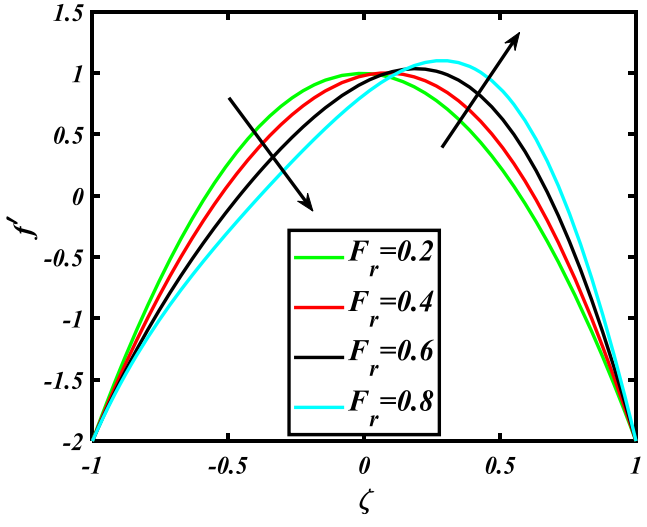

Fig. 5 Effect of F_r on f'.

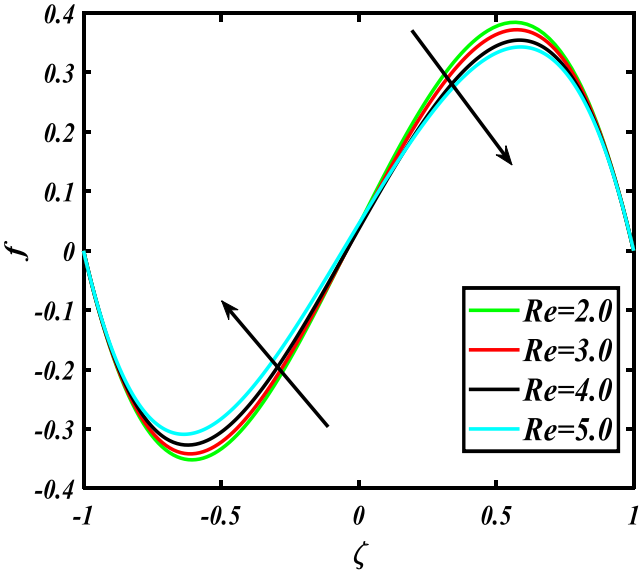

Fig. 6 Effect of Re on f.

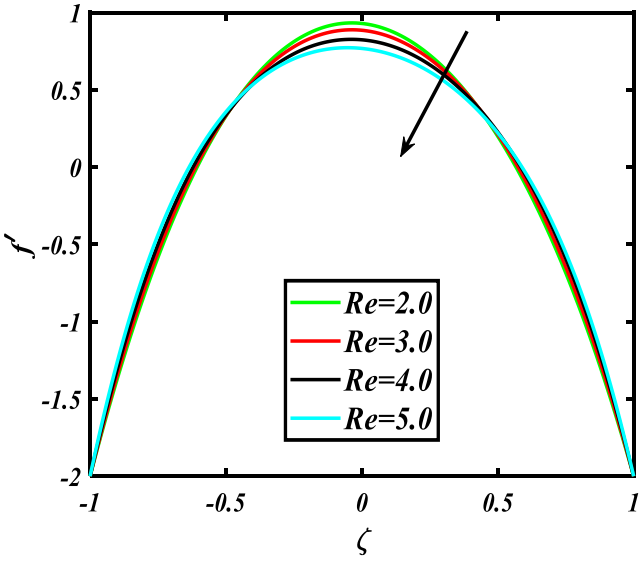

Fig. 7 Effect of Re on f'.

ble those of stationary un-stretchable disks [40]. Fig. 4 shows the micro rotational profiles of the nanofluid trending up through the plane against the increasing stretching ratio parameterγ. The increment in stretching ratio parameter directly correlates with the stretching rates of disks in radial direction so it is obvious that there must be a rise in momentum of boundary layer and the velocity profile. Fig. 5 displayed the contribution of non-uniform inertia coefficient F_r on the radial velocityf'. The radial velocity of fluid decays near the upper disk while growing near the lower disk against growing magnitudes ofF_r.

Figs. 6–8 revealed the behavior of axial, radial, and angular velocities against the stretching Reynolds numberRe. The axial velocity profile boosts near the upper disk (where $\zeta < 0$) while an opposite behavior has been detected near the lower disk (where $\zeta > 0$) as shown in Fig. 6. It is analyzed from Fig. 7 that the radial velocity field decay near the center of the plane while it grows near both disks. Fig. 8 depicted that the micromotional curves show an opposing behavior from left to the right of the plane as Re increases. The micromotional field decreases on the left side of the center of plane (near the upper disk) while showing an increasing trend on the right side of the center of plane (near the lower disk). The fluid rotates in opposite directions owing to the shear stresses, so, no (zero) microrotation locate position along disks and impact of alter rotations balanced each other.

Figs. 9–10 disclose the dependency of axial and radial velocity profiles on the bioconvection Rayleigh numberNc. The radial velocity profile deescalates (near the lower disk) with increasing Nc magnitudes while the axial velocity grows throughout the plane (from upper to the lower disk). Physically, the bioconvection Rayleigh number measures the instability between the layers of fluid due to the variation of temperature and density so that the fluid velocities are affected significantly.

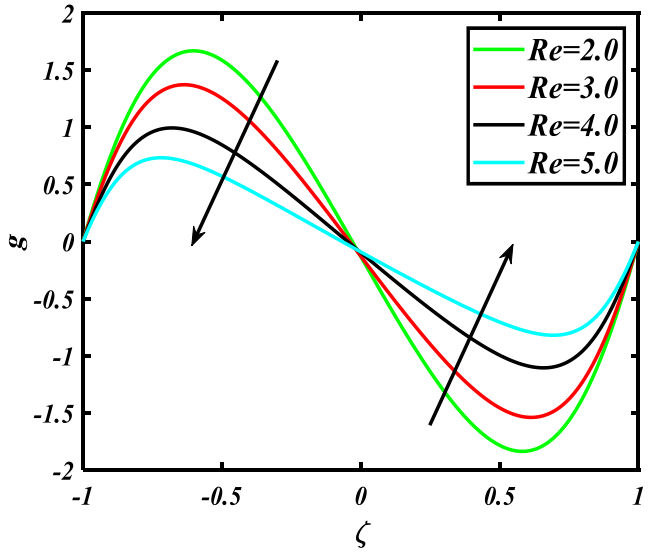

Fig. 8 Effect of Re on g.

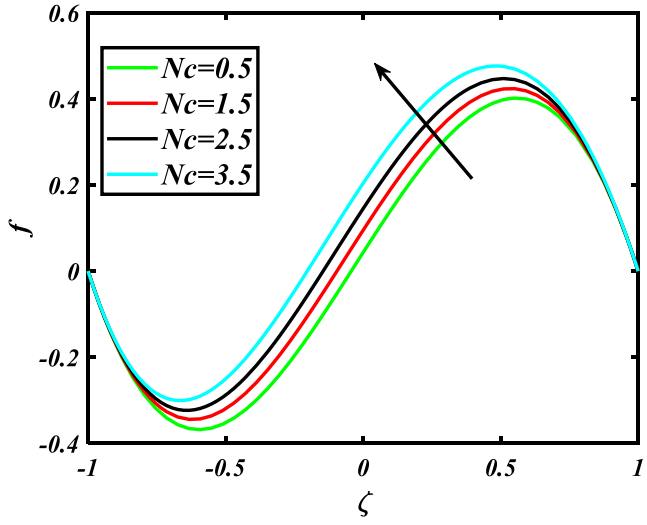

Fig. 10 Effect of Nc on f.

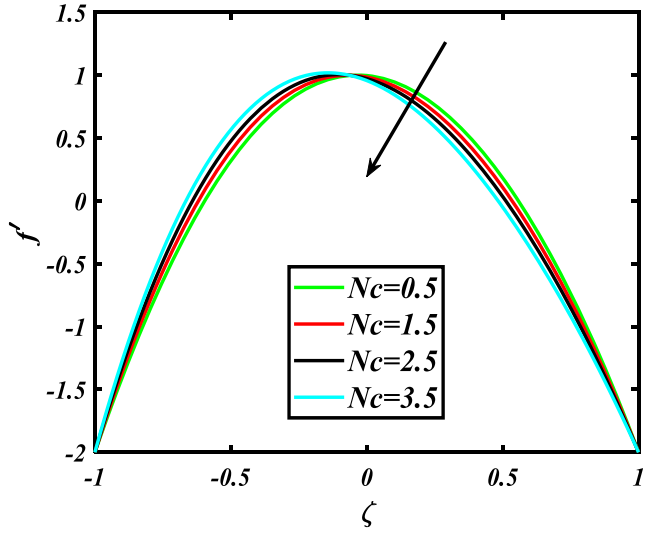

Fig. 9 Effect of Nc on f'.

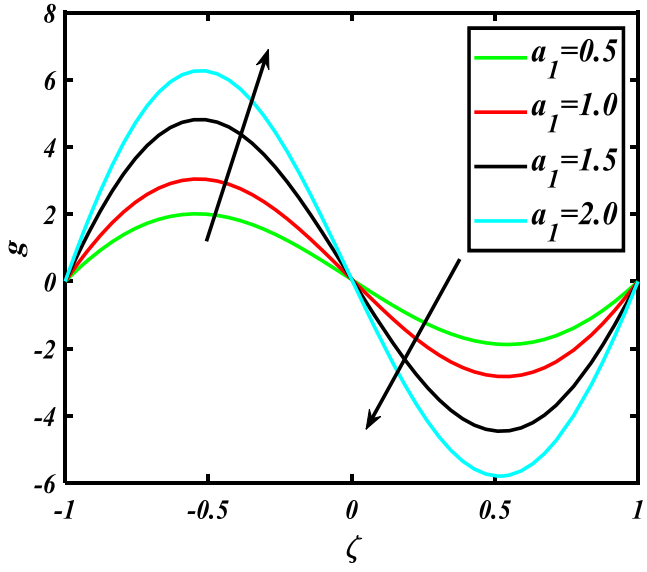

Fig. 11 Effect of a_1 on g.

Fig. 11 interprets the influence of the vortex viscosity parameter c_1 on the microrotation field$g(\zeta)$. The microrotation boosts the fluid particles in reverse directions. An opposing trend has been detected for the microrotation of fluid particles from the upper to the lower disk. For $\zeta < 0$(near the upper disk), the curve enhances while decreases for $\zeta > 0$(near the lower disk). When$c_1 = 0$, there is no microrotation of the fluid particles which also validates our numerical scheme. The magnifying values of Buoyancy ratio parameter Nr declined the radial velocity profile $f'(\zeta)$ near the lower disk as shown in Fig. 12. The physical clarification of such a decreasing trend may be attributed as the Buoyancy ratio parameter involves the buoyancy forces due to which velocity profile diminishes. The major variation in Nr results is the dominance buoyancy force related to gyrotactic motile microorganisms.

4.2. Temperature distribution

Fig. 13 elaborates the outcomes of the dimensionless temperature field $\theta(\zeta)$ versus the Prandtl numberPr. Here the temperature of nanofluid diminishes for enlarging magnitudes ofPr. Physically, the greater magnitudes of the Prandtl number produce weak heat diffusivity and consequently led to the enhanced temperature field. The effect of the Brownian motion parameter Nb against the thermal field $\theta(\zeta)$ is shown in Fig. 14. It is witnessed that the temperature field goes up against growing Nb magnitudes. Physically, larger magnitudes of the Brownian motion parameter led to the random movement of nanoparticles, and hence enhanced thermal diffusivity of the nanoparticles accelerates the thermal field of species. Fig. 15 explains the consequences of the thermal conductivity parameter ε on the dimensionless temperature field$\theta(\zeta)$. The impact

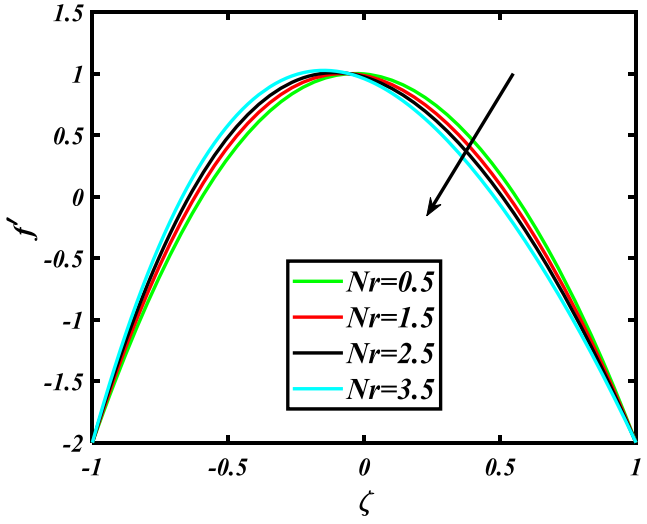

Fig. 12 Effect of Nr on f'.

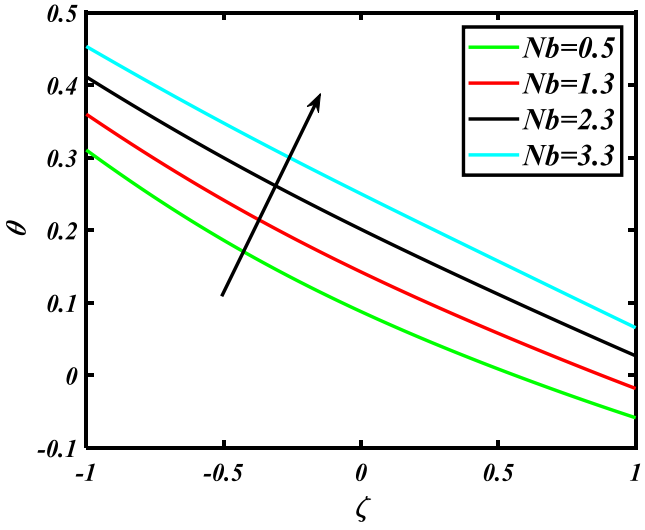

Fig. 14 Effect of Nb on θ.

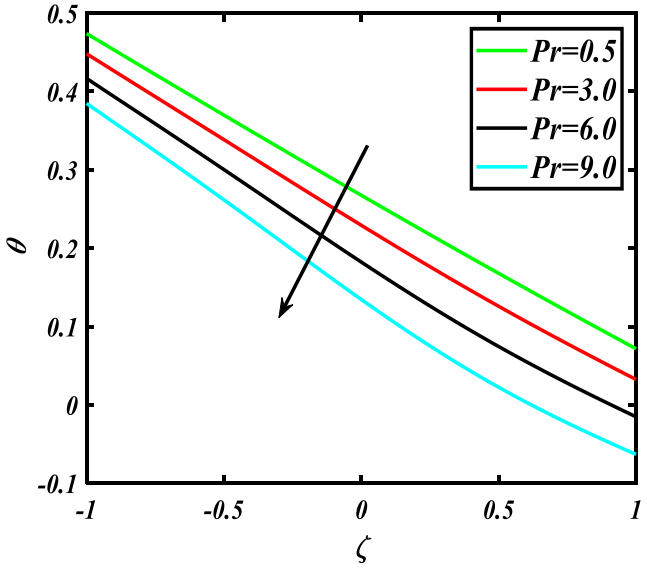

Fig. 13 Effect of Pr on θ.

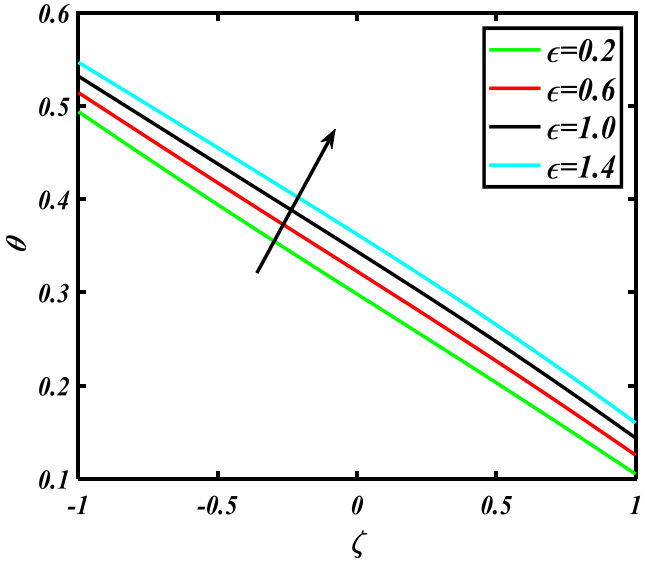

Fig. 15 Effect of ε on θ.

of temperature-dependent conductivity is more conspicuous than those of the constant conductivity. According to a physical point of view, the additional heat is transformed into the fluid through the surface of the disk. As a result, the temperature curves for the variable thermal conductivity situation are larger. The impact of the thermal Biot number Bi_1 on the solutal field of species $\theta(\zeta)$ is illustrated in Fig. 16. The increment in Bi_1 value increases the thermal field which is due to a strong convection phenomenon between the disks. The thermal Biot number for the upper disk Bi_2 shows exactly the opposite behavior than that of Bi_1 on the thermal field. The thermal field goes down with the parameter Bi_2 which is due to a weak convection phenomenon between the disks. (See Fig. 17). Thermal relaxation time parameter γ_1 outcomes are demonstrated in Fig. 18, which concluded that enlarging γ_1 values raise the temperature field. Physically, the particles need more time to transfer heat to neighboring particles, and hence thermal field of species increases. Fig. 19 explains the effects of thermal radiation Rd on the thermal fieldθ. The temperature field gets up due to the growing magnitude of the thermal radiation parameter. Physically, larger the radiation parameter led to the enhanced kinetic energy of fluid particles and hence escalates the thermal field.

4.3. Nanoparticle's concentration distribution

Figs. 20–21 are considered to discuss the effectiveness of the thermophoresis parameterNt, and the Schmidt number Sc over the dimensionless volume fraction of the nanoparticles$\phi(\zeta)$, respectively. The thermophoresis phenomenon occurs when microscopic fluid particles are drawn back from a warm to a cold location. The nanofluid particles then flow away from the heated surface, enhancing the density profile of the

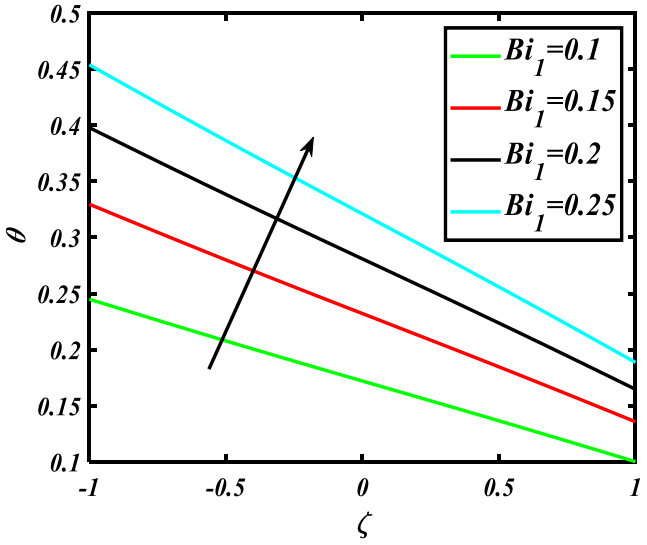

Fig. 16 effect of Bi_1 on θ.

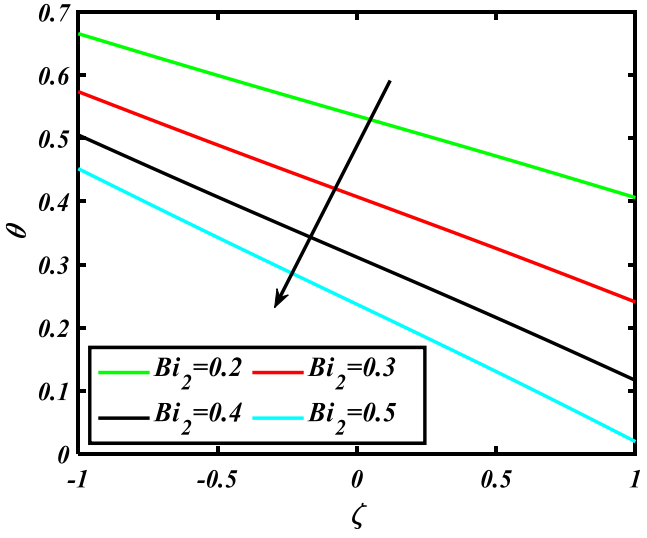

Fig. 17 Effect of Bi_2 on θ.

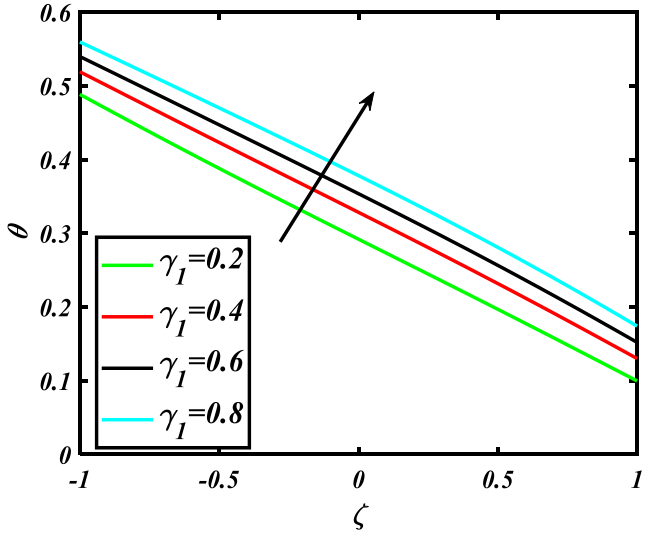

Fig. 18 Effect of γ_1 on θ.

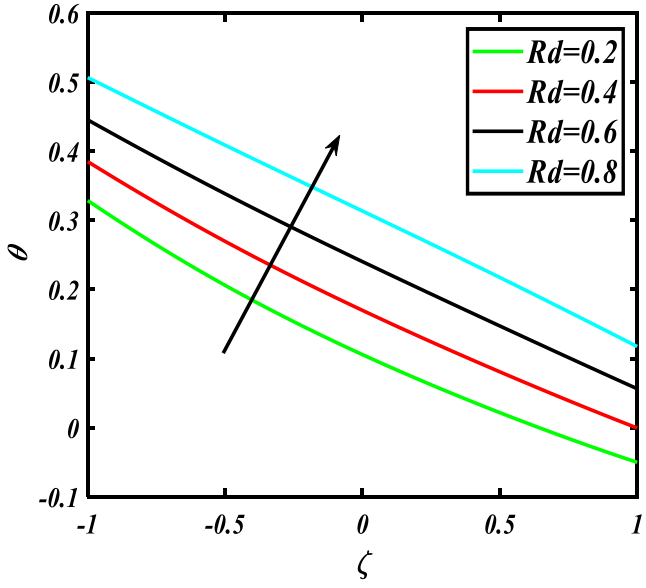

Fig. 19 Effect of Rd on θ.

nanoparticles. Fig. 21 shows that the concentration profile of nanoparticles decreases when the magnitudes of the Schmidt number Sc increases. Physically, an increment in Sc corresponds to a lower solute diffusivity which results in shorter penetration depth of concentration.

4.4. Microorganism's concentration distribution

Fig. 22 highlighted the significance of bioconvective Peclet number Pe on the dimensionless motile microorganisms' density distribution$\chi(\zeta)$. When the diffusivity of motile microorganisms reduces, then the maximum swimming speed of microorganisms' cells also deccreases. This is the physical fact that the microorganisms' density distribution also reduces when the bioconvection Peclet number increases. Fig. 23 reports the influence of bioconvection Lewis number Lb on the dimensionless motile microorganisms' density distribution$\chi(\zeta)$. It can be inferred that the positive fluctuations in the bioconvection Lewis number reduce the motile microorganisms' profile. Physically, as the value of Lb increases, the rate of viscous diffusion increases, and hence the density profile of motile microorganisms in the boundary layer decreases.

Table 1 represents the impacts ofλ, Nr, Nc, a_1, Re, γ, and F_r parameters on Shear and couple stresses at the upper and lower disks, respectively. Enhancing magnitudes of mixed convection parameter λ reduces the shear stresses f'' while boosting the couple stressesg'. Buoyancy ratio parameter Nr and bioconvective Rayleigh number Nc cause an improvement in shear stresses; however, a decline in couple stresses has been noticed. Shear and couple stresses are enhanced by the vortex

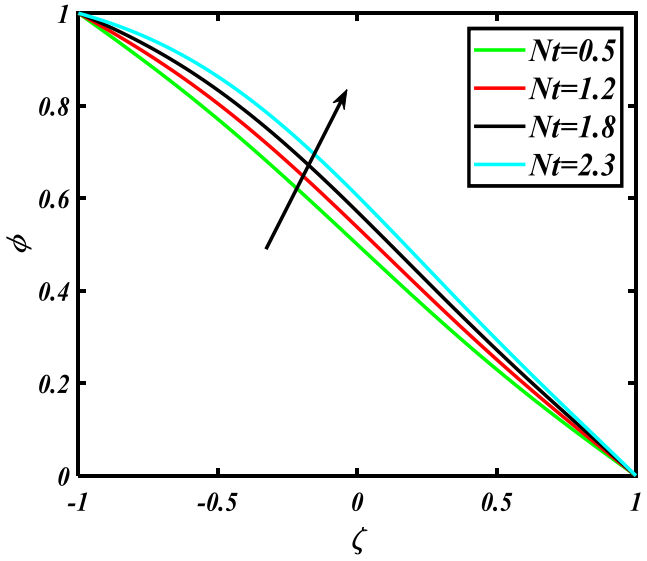

Fig. 20 Effect of Nt on ϕ.

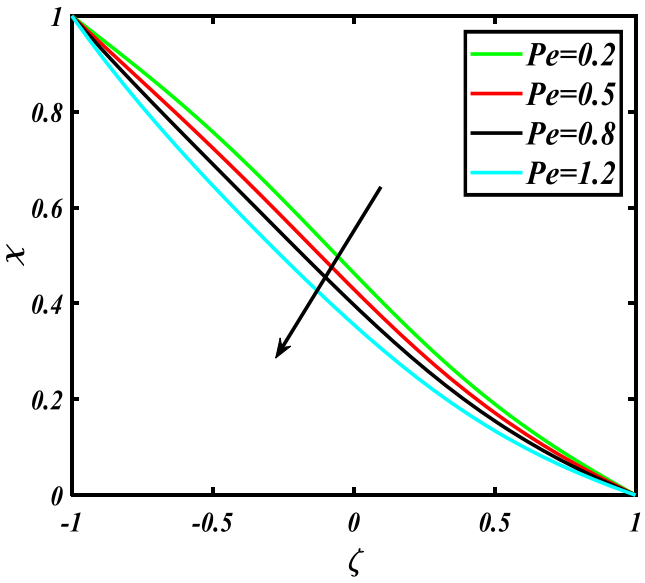

Fig. 22 Effect of Pe on χ.

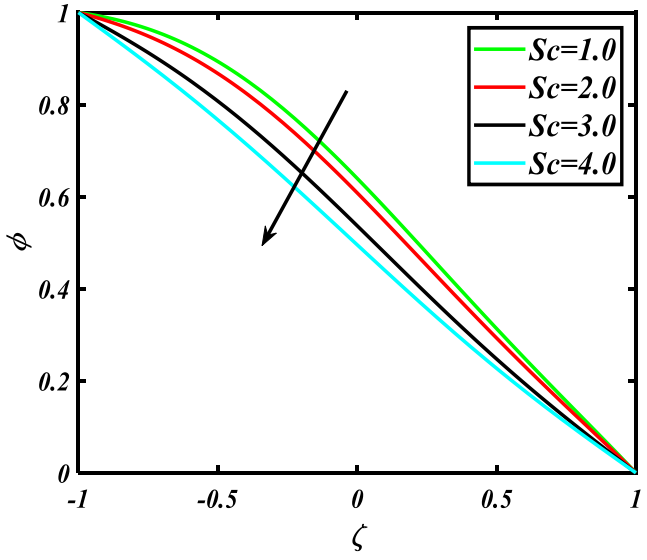

Fig. 21 Effect of Sc on ϕ.

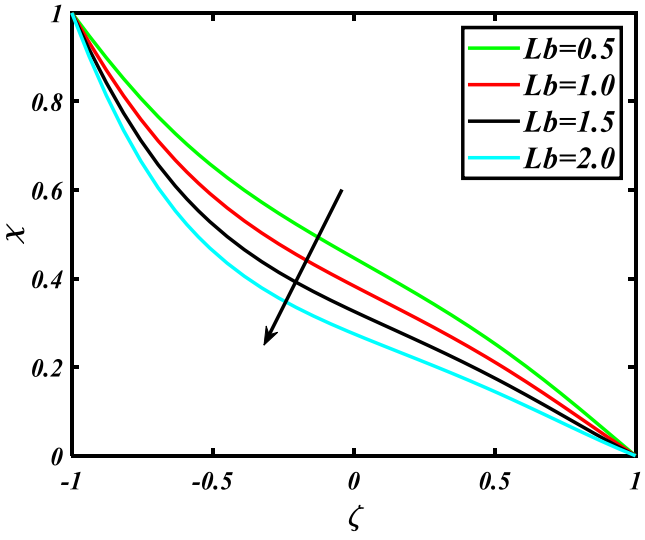

Fig. 23 Effect of Nt on χ.

Table 1 Shear and couple stresses for the parameters λ, Nr, Nc, a_1, Re, γ, and F_r.

λ	Nr	Nc	a_1	Re	γ	F_r	$f''(1)$	$-f''(-1)$	$g'(1)$	$g'(-1)$
0.3	0.1	0.1	0.5	0.3	1.0	0.1	12.0333	1.8661	5.4670	16.6525
0.7							12.0272	11.8664	5.4684	16.6656
1.2							12.0203	11.8730	5.4701	16.6821
1.8							12.0116	11.8810	5.4722	16.7018
0.1	0.2	0.1	0.5	0.3	1.0	0.1	12.0365	11.8583	5.4663	16.6456
	0.4						12.0372	11.8578	5.4662	16.6448
	0.6						12.0379	11.8574	5.4660	16.6440
	0.8						12.0385	11.8570	5.4659	16.6432
0.1	0.1	0.5	0.5	0.3	1.0	0.1	12.0368	11.8581	5.4662	16.6452
		1.0					12.0385	11.8570	5.4659	16.6433
		1.5					12.0401	11.8559	5.4656	16.6414
		2.0					12.0417	11.8548	5.4653	16.6395
0.1	0.1	0.1	0.4	0.3	1.0	0.1	12.0259	12.0063	4.2935	4.3030
			0.7				12.0625	11.9697	7.9245	8.0564
			1.0				12.0803	11.8920	15.3116	10.5243
			1.3				12.1767	11.8333	17.7304	16.5681
0.1	0.1	0.1	0.5	1.0	1.0	0.1	12.2261	12.0437	17.6672	5.5066
				2.0			12.2805	12.1153	17.6442	5.5311
				3.0			12.3345	12.1878	17.6454	5.5570
				4.0			12.3882		17.6582	
0.1	0.1	0.1	0.5	0.3	0.3	0.1	9.4748	9.2480	1.7879	6.8277
					0.6		10.6389	10.4290	8.7654	6.2557
					0.9		11.8009	11.6039	15.5118	5.6814
					1.2		12.9607	12.7726	22.0375	5.1049
0.1	0.1	0.1	0.5	0.3	1.0	0.3	12.1848	11.9985	17.7019	5.4880
						0.7	12.1791	12.0077	17.6835	5.4851
						1.1	12.1734	12.0161	17.6652	5.4822
						1.8	12.1633		17.6331	

Table 2 Heat flux for the parameters Pr, Nt, Nb, λ, Nr, Bi_1, Bi_2, Re, and γ.

Pr	Nt	Nb	λ	Nr	Bi_1	Bi_2	Re	γ	$\theta'(1)$	$\theta'(-1)$
0.5	0.1	0.3	0.1	0.1	0.4	0.3	0.3	1.0	0.1696	−0.1788
1.0									−0.1712	−0.1830
1.5									−0.1727	−0.1872
2.0									−0.1743	−0.1915
1.2	0.4	0.3	0.1	0.1	0.4	0.3	0.3	1.0	−0.1753	−0.1885
	0.8								−0.1766	−0.1845
	1.2								−0.1780	−0.1805
	1.6								−0.1794	−0.1767
1.2	0.1	0.4	0.1	0.1	0.4	0.3	0.3	1.0	−0.1763	−0.1974
		0.8							−0.1843	−0.2214
		1.2							−0.1924	−0.2454
		1.6							−0.2006	−0.2685
1.2	0.1	0.3	0.3	0.1	0.4	0.3	0.3	1.0	−0.1743	−0.1915
			0.7						−0.1645	−0.1912
			1.2						−0.1543	−0.1909
			1.8						−0.1434	−0.1901
1.2	0.1	0.3	0.1	0.2	0.4	0.3	0.3	1.0	−0.1743	−0.1915
				0.4					−0.1734	−0.1815
				0.6					−0.1723	−0.1705
				0.8					−0.1711	−0.1675
1.2	0.1	0.3	0.1	0.1	0.5	0.3	0.3	1.0	−0.1905	−0.2117
					1.0				−0.2339	−0.2686
					1.5				−0.2529	−0.2950
					2.0				−0.2636	−0.3102

(*continued on next page*)

Table 2 (*continued*)

Pr	Nt	Nb	λ	Nr	Bi_1	Bi_2	Re	γ	$\theta'(1)$	$\theta'(-1)$
1.2	0.1	0.3	0.1	0.1	0.4	0.4	0.3	1.0	−1.0658	−0.2208
						1.0			−1.0660	−0.3032
						1.6			−1.0662	−0.3339
						2.2			−1.0663	−0.3498
1.2	0.1	0.3	0.1	0.1	0.4	0.3	1.0	1.0	−0.2320	−0.2312
							2.0		−0.2926	−0.2862
							3.0		−0.3382	−0.3308
							4.0		−0.3366	
1.2	0.1	0.3	0.1	0.1	0.4	0.3	0.3	0.3	−0.1939	−0.1982
								0.6	−0.1908	−0.1952
								0.9	−0.1877	−0.1923
								1.2	−0.1847	−0.1893

Table 3 Mass flux for the parameters Pr, Nt, Nb, λ, Nr, Re, γ, F_r, and Sc.

Pr	Nt	Nb	λ	Nr	Re	γ	F_r	Sc	$\phi'(1)$	$\phi'(-1)$
0.5	0.1	0.3	0.1	0.1	0.3	1.0	0.1	2.0	−1.0676	1.0745
1.0									−1.0671	1.0761
1.5									−1.0665	1.0778
2.0									−1.0659	1.0795
1.2	0.4	0.3	0.1	0.1	0.3	1.0	0.1	2.0	−1.0608	1.0984
	0.8								−1.0511	1.1145
	1.2								−1.0379	1.1203
	1.6								−1.0212	1.1263
1.2	0.1	0.4	0.1	0.1	0.3	1.0	0.1	2.0	−1.0657	1.0791
		0.8							−1.0655	1.0786
		1.2							−1.0652	1.0786
		1.6							−1.0653	1.0787
1.2	0.1	0.3	0.3	0.1	0.3	1.0	0.1	2.0	−1.0659	1.0794
			0.7						−1.0661	1.0793
			1.2						−1.0662	1.0792
			1.8						−1.0664	1.0790
1.2	0.1	0.3	0.1	0.2	0.3	1.0	0.1	2.0	−1.0659	1.0795
				0.4					−1.0539	1.0655
				0.6					−1.0435	1.0615
				0.8					−1.0232	1.0597
1.2	0.1	0.3	0.1	0.1	1.0	1.0	0.1	2.0	−1.0389	1.0928
					2.0				−1.0114	1.1177
					3.0				−0.9879	1.1401
					4.0				−0.9710	
1.2	0.1	0.3	0.1	0.1	0.3	0.3	0.1	2.0	−1.1571	1.1785
						0.6			−1.1141	1.1344
						0.9			−1.0715	1.0907
						1.2			−1.0292	1.0474
1.2	0.1	0.3	0.1	0.1	0.3	1.0	0.3	2.0	−1.0574	1.0761
							0.7		−1.0575	1.0758
							1.1		−1.0577	1.0756
							1.8		−1.0579	
1.2	0.1	0.3	0.1	0.1	0.3	1.0	0.1	3.0	−1.0905	1.1117
								4.0	−1.1235	1.1477
								5.0	−1.1569	1.1844
								6.0	−1.1908	1.2217

viscosity parametera_1. Due to the Stretching Reynolds number Re and stretching ratio parameterγ, the shear stresses are increased near the upper disk while showing an opposite behavior near the lower disk. Similarly, an opposite trend can be noticed for the same parameters on couple stresses near upper and lower disks, respectively. The inertia coefficient (Darcy-Forchheimer parameter)F_r reduces the shear and couple stresses.

Table 2 represents the impacts of parametersPr, Nt, Nb, λ, Nr, Bi_1, Bi_2, Re, and γ on the local Nusselt number that measures the heat flux. It can be analyzed from the table data that the heat transfer rate θ' declined against the growing values of Prandtl number, thermal Biot numbers, and the Reynolds number at the upper and lower disks, respectively. The mixed convection parameter, Buoyancy ratio parameter, and stretching ratio parameter accelerate the heat transfer rate.

The mass transfer rate is discussed with the help of numerical data given in Table 3. Prandtl number Pr and thermophoretic parameter Nt improves the mass transfer rate whereas mass transportation rate is reduced for larger mixed convection parameter λ amount at both upper and lower disks, respectively. The rate of mass transportation is decayed against growing Nb, Nr, Re, γ and F_r values at the upper disk while an opposite trend can be noticed at the lower disk. The enlarging Schmidt number Sc values retard the mass transportation at the upper disc.

Table 4 illustrates the scenario of how the microorganisms rate variate for enhanced values of the parametersPe, Lb, λ, Nr, Re, γ, andF_r. The Peclet number Pe and the bioconvection Lewis number Lb enhance the microorganisms' rate at the lower disk whereas the stretching ratio parameter γ and the Buoyancy ratio parameter Nr at the upper disk, respectively. The mixed convection parameter λ and the inertia coefficient (Darcy-Forchheimer parameter)F_r lead to a decrease in the microorganisms' concentration rate. Table 5 indicates the comparative analysis of our current numerical results with previous published work. From Table 5, it can be observed a good agreement between our numerical outcomes and previous work under limiting scenario.

Table 4 Microorganism flux for the parameters Pe, Lb, λ, Nr, Re, γ, and F_r.

Pe	Lb	λ	Nr	Re	γ	F_r	$\chi'(1)$	$\chi'(-1)$
0.5	2.0	0.1	0.1	0.3	1.0	0.1	−1.3850	1.3997
1							−1.7473	1.7725
1.5							−2.1467	2.1827
2							−2.5781	2.6249
0.1	3	0.1	0.1	0.3	1.0	0.1	−1.1591	1.1684
	4						−1.1941	1.2062
	5						−1.2295	1.2446
	6						−1.2653	1.2836
0.1	2.2	0.3	0.1	0.3	1.0	0.1	−1.1289	1.1349
		0.7					−1.1290	1.1348
		1.2					−1.1291	1.1346
		1.8					−1.1293	1.1345
0.1	2.0	0.1	0.2	0.3	1.0	0.1	−1.1288	1.1350
			0.4				−1.1276	1.1231
			0.6				−1.1165	1.1132
			0.8				−1.0856	1.1013
0.1	2.0	0.1	0.1	1.0	1.0	0.1	−1.1220	1.1330
				2.0			−1.1189	1.1355
				3.0			−1.1162	1.1377
				4.0			−1.1142	
0.1	2.0	0.1	0.1	0.3	0.3	0.1	−1.2373	1.2430
					0.6		−1.1885	1.1949
					0.9		−1.1401	1.1472
					1.2		−1.0920	1.0998
0.1	2.0	0.1	0.1	0.3	1.0	0.3	−1.1242	1.1312
						0.7	−1.1243	1.1310
						1.1	−1.1244	1.1307
						1.8	−1.1247	

Table 5 A Comparative result of ReC_f and ReC_g for different values of M with previous work under limiting case.

M	Ali *et al.* [40]	Siddiq *et al.* [42]	Current	Ali *et al.* [42]	Siddiq *et al.* [42]	Current
	ReC_f	ReC_f	ReC_f	ReC_g	ReC_g	ReC_g
0	10.5522	10.5522	10.5522	1.2595	1.2595	1.2595
0.5	11.4483	11.4482	11.4483	1.2816	1.2817	1.2816
1.0	13.7080	13.7081	13.7082	1.3347	1.3346	1.3348
1.5	16.6320	16.6320	16.6319	1.3970	1.3971	1.3969
2.0	19.8207	19.8208	19.8208	1.4560	1.4560	1.4560

5. Conclusions

In the current article, the Darcy-Forchheimer impacts in a micropolar nanofluid flow in the presence of gyrotactic microorganisms between two coaxial, parallel, and radially stretching disks with convective thermal boundary conditions were examined. The effects of heat conductivity and thermal radiations were also considered for this flow. The influence of gyrotactic microorganisms was accommodated through the bioconvection phenomenon. The Cattaneo-Christov heat flux theory was also implemented. The major concluding remarks were summarized below:

- The axial and micro rotational velocities depict an increasing trend throughout the central plane from the upper to the lower disk against increasing values of stretching ratio parameterγ.
- The radial velocity increases near the upper disk and decreases near the lower disk against enlarging values of the stretching ratio parameterγ.
- The radial velocity decreases near the upper disk and increases near the lower disk for the growing magnitudes of inertia coefficientF_r.
- The bioconvection Rayleigh number Nc and the buoyancy ratio parameter Nr deaccelerate the radial velocity f' near the lower disk.
- The vortex viscosity parameter a_1 enhances the microrotation field near the upper disk while diminishing it near the lower disk.
- The thermal profile θ accelerates throughout the central plane against the thermal radiationRd, thermal conductivity parameterε, thermal Biot numberBi_1, and for Brownian motion parametersNb.
- The nanoparticles density profile ϕ is boosted-up throughout the central plane against the thermophoresis parameter Nt while declined for Schmidt numberSc.
- The gyrotactic motile microorganisms' density profile χ is de-escalated throughout the central plane for both the Peclet number Pe and the bioconvection Lewis numberLb.
- Micropolar parameters cause increment of couple stresses and a decrement in shear stresses.

Declaration of Competing Interest

The authors declare that they have no known competing financial interests or personal relationships that could have appeared to influence the work reported in this paper.

Acknowledgments

The authors extend their appreciation to the Deanship of Scientific Research at King Khalid University for funding this project under grant number (RGP.2/238/43). The authors express their appreciation to the Deputyship for Research & Innovation, Ministry of Education, in Saudi Arabia, for funding this research work through the project number: (IFP-KKU-2020/10). This work is financially supported by the Government College University, Faisalabad, and Higher Education Commission, Pakistan.

References

[1] V.B. Awati, M. Jyoti, N.M. Bujurke, Series solution of steady viscous flow between two porous disks with stretching motion, J. Nanofluids 7 (2018) 982–994.
[2] I. Khan, K.U. Rehamn, M.Y. Malik, et al, On magnetized non-Newtonian rotatory fluid flow field, Adv. Mech. Eng. 11 (2019) 1–12.
[3] A. Das, Analytical solution to the flow between two coaxially rotating disk, Procedia Eng. 127 (2015) 377–382.
[4] M. Turkyilmazoglu, Flow and heat simultaneously induced by two stretchable disks, Phys. Fluids 28 (2016) 043601.
[5] T. Hayat, S. Qayyum, M. Imtiaz, et al, MHD flow and heat transfer between coaxially rotating disks in a thermally stratified medium, PLoS ONE 11 (2016) 1–23.
[6] A.C. Eringen, Micropolar fluids with stretch, Int. J. Eng. Sci. 7 (1) (1969) 115–127.
[7] M. Ashraf, M.A. Kamal, K.S. Syed, Numerical simulation of flow of a micropolar fluid between a porous disk and a non-porous disk, Appl. Math. Model 33 (2009) 1933–1943.
[8] M. Ashraf, A.R. Wehgal, MHD flow and heat transfer of micropolar fluid between two porous disks, Appl. Math. Mech. 33 (2012) 51–64.
[9] K. Ali, S. Ahmad, K. Ali, Numerical simulation of flow and heat transfer in hydromagnetic micropolar fluid between two stretchable disks with viscous dissipation effects, J. Theor. Mech. 54 (2016) 633–643.
[10] S.S. Ghadikolaei, K. Hosseinzadeh, M. Hatami, et al, MHD boundary layer analysis for micropolar dusty fluid containing hybrid nanoparticles Cu-Al2O3 over a porous medium, J. Mol. Liq. 268 (2018) 813–823.
[11] V. Tailor, M. Goyal, Effect of magnetic field on free convective micropolar fluid flow with radiation and heat source over a shrinking sheet, SSRN 3446604, 2019.
[12] R. Mehmood, S. Nadeem, S. Masood, Effects of transverse magnetic field on a rotating micropolar fluid between parallel plates with heat transfer, J. Magn. Magn. Mater. 401 (2016) 1006–1014.
[13] K.A. Kumar, V. Sugunamma, N. Sandeep, M. Mustafa, Simultaneous solutions for first order and second order slips on micropolar fluid flow across a convective surface in the presence of Lorentz force and variable heat source/sink, Sci. Rep. 9 (1) (2019 Oct 11) 1–4.
[14] K. Anantha Kumar, V. Sugunamma, N. Sandeep, Influence of viscous dissipation on MHD flow of micropolar fluid over a slendering stretching surface with modified heat flux model, J. Therm. Anal. Calorim. 139 (6) (2020 Mar) 3661–3674.
[15] A.C. Venkata Ramudu, K. Anantha Kumar, V. Sugunamma, N. Sandeep, Impact of Soret and Dufour on MHD Casson fluid flow past a stretching surface with convective–diffusive conditions, J. Therm. Anal. Calorim. 6 (2021 Feb) 1.
[16] N. Sandeep, B. Ranjana, S.P. Samrat, G.P. Ashwinkumar, Impact of nonlinear radiation on magnetohydrodynamic flow of hybrid nanofluid with heat source effect, Proc. Instit. Mech. Eng., Part E: J. Process Mech. Eng. (2022), Jan 18:09544089211070667.
[17] K.A. Kumar, V. Sugunamma, N. Sandeep, S. Sivaiah, Physical aspects on MHD micropolar fluid flow past an exponentially stretching curved surface, InDefect and Diffusion Forum, Vol. 401, Trans Tech Publications Ltd, 2020, pp. 79–91.
[18] P.K. Pattnaik, M.M. Bhatti, S.R. Mishra, M.A. Abbas, O.A. Bég, Mixed convective-radiative dissipative magnetized micropolar nanofluid flow over a stretching surface in porous media with double stratification and chemical reaction effects: ADM-Padé computation, J. Math. 25 (2022 Jan) 2022.
[19] M.M. Bhatti, O.A. Bég, S.I. Abdelsalam, Computational Framework of Magnetized MgO–Ni/Water-Based Stagnation

Nanoflow Past an Elastic Stretching Surface: Application in Solar Energy Coatings, Nanomaterials. 12 (7) (2022) 1049.
[20] H. Zhang, X. Nie, D.O. Bokov, D. Toghraie, O.A. Akbari, F. Montazerifar, F. Pourfattah, Y. Esmaeili, R. Khodaparast, Numerical study of mixed convection and entropy generation of Water-Ag nanofluid filled semi-elliptic lid-driven cavity, Alexandria Eng. J.. 61 (11) (2022) 8875–8896.
[21] K. Eric Drexler, Engines of Creation: The Coming Era of Nanotechnology, Doubleday, 1986 (ISBN 978-0-385-19973-5).
[22] S.U.S. Choi, Enhancing thermal conductivity of fluids with nanoparticles. In: International mechanical engineering congress and exposition, San Francisco, USA, ASME, FED 231/MD, 66, 99–105 (1995).
[23] J. Buongiorno, Convective transport in nanofluids, ASME J. Heat Transf. 128 (2006) 240–250.
[24] M. Waqas, M.I. Khan, T. Hayat, M.M. Gulzar, A. Alsaedi, Transportation of radiative energy in viscoelastic nanofluid considering buoyancy forces and convective conditions, Chaos; Solitons Fractals 130 (2020) 109415.
[25] K. Jyothi, P.S. Reddy, M.S. Reddy, Influence of magnetic field and thermal radiation on convective flow of SWCNTs-water and MWCNTs-water nanofluid between rotating stretchable disks with convective boundary conditions, Powder Tech 331 (2018) 326–337.
[26] A. Rauf, Z. Abbas, S.A. Shehzad, Utilization of Maxwell-Cattaneo law for MHD swirling flow through oscillatory disk subject to porous medium, Appl. Math. Mech. 40 (2019) 837–850.
[27] T. Hayat, S. Qayyum, S.A. Shehzad, et al, Cattaneo-Christov double-diffusion theory for three-dimensional flow of viscoelastic nanofluid with the effect of heat generation/absorption, Results Phys. 8 (2018) 489–495.
[28] S.A. Shehzad, S.U. Khan, Z. Abbas, A. Rauf, A revised Cattaneo-Christov mi-cropolar viscoelastic nanofluid model with combined porosity and magnetic effects, Appl. Math. Mech. (English Edition) 41 (3) (2020) 521{532, https://doi.org/10.1007/s10483-020-2581-5.
[29] A. Rauf, Z. Abbas, S.A. Shehzad, Utilization of Maxwell-Cattaneo law for MHD swirling flow through oscillatory disk subject to porous medium, Appl. Math. Mech. (English Edition) 40 (6) (2019) 837{850, https://doi.org/10.1007/s10483-019-2488-9.
[30] S.M. Upadhya, C.S.K. Raju, Mahesha, S. Saleem, Nonlinear unsteady convection on micro and nanofluids with Cattaneo-Christov heat flux, Results Phys. 9 (2018) 779–786.
[31] L. Liu, L. Zheng, F. Liu, X. Zhang, Heat conduction with fractional Cattaneo-Christov upper-convective derivative heat flux, Int. J. Therm. Sci. 112 (2017) 421–426.
[32] M. Tabassum, M. Mustafa, Numerical treatment for partial slip flow and heat transfer of non-Newtonian Reiner-Rivlin fluid due to rotating disk, Int. J. Heat Mass Transf. 123 (2018) 979–987.
[33] B.J. Gireesha, M.R. Krishnamurthy, K. Ganeshkumar, Nonlinear radiative heat transfer and boundary layer flow of Maxwell nanofluid past stretching sheet, J. Nanofluids 8 (5) (2019) 1093–1102.
[34] J.R. Platt, " Bioconvection Patterns" in Cultures of Free-Swimming Organisms, Science 133 (3466) (1961) 1766–1767.
[35] A.V. Kuznetsov, Bio-thermal convection induced by two different species of microorganisms, Int. Commun. Heat Mass Transfer 38 (5) (2011) 548–553.
[36] S.U. Khan, I. Tlili, Significance of activation energy and effective Prandtl number in accelerated flow of Jeffrey nanoparticles with gyrotactic microorganisms, J. Energy Res. Technol. 142 (11) (2020).
[37] T. Hayat, Z. Bashir, S. Qayyum, A. Alsaedi, Nonlinear radiative flow of nanofluid in presence of gyrotactic microorganisms and magnetohydrodynamic, Int. J. Numer. Meth. Heat Fluid Flow (2019).
[38] Z. Abdelmalek, S.U. Khan, H. Waqas, K. Al-Khaled, I. Tlili, A proposed unsteady bioconvection model for transient thin film flow of rate-type nanoparticles configured by rotating disk, J. Therm. Anal. Calorim. 144 (5) (2021) 1639–1654.
[39] Z. Abbas, T. Mushtaq, S.A. Shehzad, et al, Slip flow of hydromagnetic micropolar nanofluid between two disks with characterization of porous medium, J. Braz. Soc. Mech. Sci. Eng. 41 (2019) 465.
[40] K. Ali, S. Ahmad, M. Ashraf, On combined effect of thermal radiation and viscous dissipation in hydromagnetic micropolar fluid flow between two stretchable disks, Thermal. Sci. 21 (2017) 2155–2166.
[41] B. Kumar, G.S. Seth, M.K. Singh, et al, Carbon nanotubes (CNTs)-based flow between two spinning discs with porous medium, Cattaneo-Christov (non-Fourier) model and convective thermal condition, J. Therm. Anal. Calorim. 146 (2021) 241–252.
[42] M.K. Siddiq, M. Ashraf, Bioconvection of micropolar nanofluid with modified Cattaneo-Christov theories, Adv. Mech. Eng. 12 (5) (2020), 1687814020925217.